ACS OMEGA

http://pubs.acs.org/journal/acsodf

Article

Superconducting Gap of Pressure Stabilized $(Al_{0.5}Zr_{0.5})H_3$ from *Ab Initio* Anisotropic Migdal−Eliashberg Theory

Prutthipong Tsuppayakorn-aek, Rajeev Ahuja, Thiti Bovornratanaraks,* and Wei Luo

Cite This: *ACS Omega* 2022, 7, 28190−28197

Read Online

ACCESS | Metrics & More | Article Recommendations

ABSTRACT: Motivated by Matthias' sixth rule for finding new superconducting materials in a cubic symmetry, we report the cluster expansion calculations, based on the density functional theory, of the superconducting properties of $Al_{0.5}Zr_{0.5}H_3$. The $Al_{0.5}Zr_{0.5}H_3$ structure is thermodynamically and dynamically stable up to at least 200 GPa. The structural properties suggest that the $Al_{0.5}Zr_{0.5}H_3$ structure is a metallic. We calculate a superconducting transition temperature using the Allen−Dynes modified McMillan equation and anisotropic Migdal−Eliashberg equation. As result of this, the anisotropic Migdal−Eliashberg equation demonstrated that it exhibits superconductivity under high pressure with relatively high-T_c of 55.3 K at a pressure of 100 GPa among a family of simple cubic structures. Therefore, these findings suggest that superconductivity could be observed experimentally in $Al_{0.5}Zr_{0.5}H_3$.

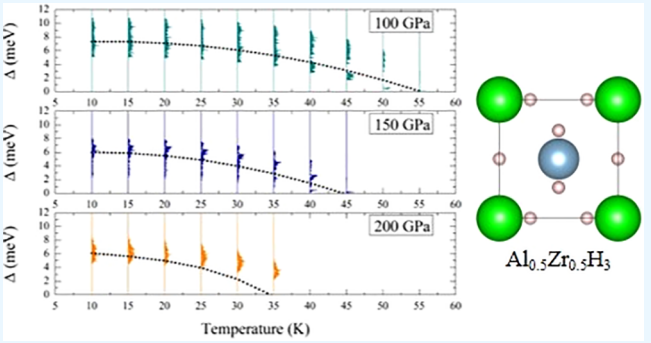

INTRODUCTION

Motivated by the discovery of the intermetallic superconductor Nb_3Sn in 1954, its superconducting transition temperature (T_c) was found by Matthias et al.[1] to be T_c of 18 K. In addition, in 1973, the intermetallic compound Nb_3Ge was reported by Gavaler to superconduct with T_c up to 22 K.[2] The superconductivity of intermetallics has encountered high T_c, but their T_c cannot overtake the boiling point of nitrogen at 77 K. In 1968, the work of Ashcroft was beginning to reveal that hydrogen became a metallic state.[3] Following this prediction, hydrogen in a metallic state can achieve a high T_c, as suggested by Gilman[4] Interestingly, the phenomenon of the superconductivity of metallic hydrogen can be described by the Bardeen−Cooper−Schrieffer (BCS) theory[5] based on phonon-mediated superconductivity. In 2004, the potential of hydrogen further indicated that it is a dominant component for alloys of metallic hydrogen[6] because of the considerable increase in the electron−phonon coupling (EPC).

In a great success for BCS theory and the prediction of Ashcroft, the discoveries of high T_c for metal hydrides have since been experimentally observed; moreover, metal hydrides have been theoretically predicted to have high T_c.[7−22] Recently, an isostructural family of A15 was reported in AlH_3 and ZrH_3.[23,24] It is interesting to note that both AlH_3 and ZrH_3 are isostructural to Nb_3Sn and Nb_3Ge with $Pm\bar{3}n$ symmetry. Also, these structures turn out to be superconductors at high pressure. To clarify, AlH_3 attracted interest because of a discrepancy between theoretical and experimental findings.[25] It should be mentioned that the contradiction of superconductivity in AlH_3 was investigated by Abe,[23] and it was revealed to superconduct at pressures above 100 GPa. Also, its T_c is theoretically predicted to be 28.5 K at a pressure of 105 GPa[23] and 24 K at a pressure of 110 GPa.[25] For ZrH_3, very recently, it was explored in detail theoretically by predicting a crystal structure at 1 atm and 50 and 100 GPa. As a result of this, the $Pm\bar{3}n$ symmetry is thermodynamically stable up to at least 100 GPa. Besides, ZrH_3 was successfully synthesized in detail experimentally in diamond anvil cells by two different reaction routes.[24] These findings tempt one to examine its T_c. In short, the T_c of ZrH_3 is reported to be 6.4 K at a pressure of 40 GPa according to the aforementioned experimental findings[24,25] and recent extensive studies.[23−25] It is also worth paying attention to the prospective structure because it has suitable abilities to carry out superconductivity of Al/Zr-substituted metal trihydride at high pressure. In particular, the structure effectively predicted a T_c within the same theoretical framework employed here.

Therefore, in this paper, Al/Zr-substituted metal trihydride is investigated by using a cluster expansion (CE) based on density functional theory. Equally important, as mentioned

Received: April 19, 2022
Accepted: June 30, 2022
Published: August 1, 2022

ACS Publications

© 2022 The Authors. Published by American Chemical Society

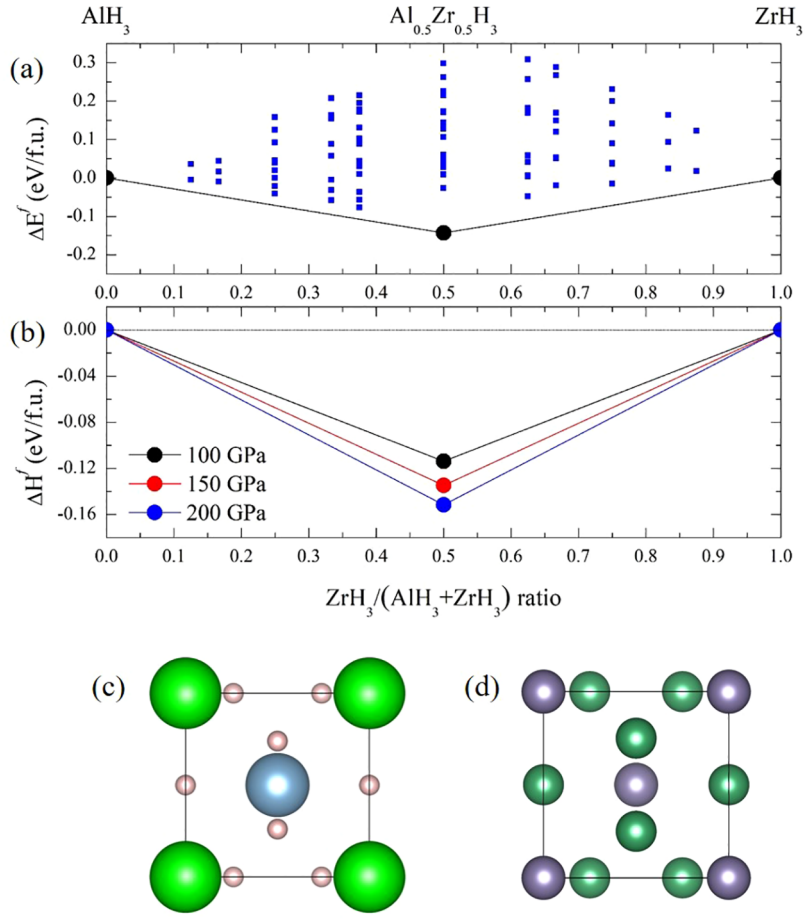

Figure 1. (a) First-principles formation energies are predicted up to 92 structures (solid dark blue squares), evaluated with respect to $Pm\bar{3}n$-AlH_3 and $Pm\bar{3}n$-ZrH_3 structures. The black solid circles, connected by thick black lines, represents the $Pm\bar{3}n$-AlH_3, $Pm\bar{3}n$-ZrH_3, and $Pm\bar{3}$-$Al_{0.5}Zr_{0.5}H_3$. (b) First-principles formation enthalpy of $Pm\bar{3}$-$Al_{0.5}Zr_3H_3$ as a function of pressure ranging from 100 to 200 GPa. (c) Schematic illustration of the $Pm\bar{3}$-$Al_{0.5}Zr_{0.5}H_3$ structure; the Al atoms are shown in light blue, the Zr atoms in green, and the H atoms in pink. (d) Schematic illustration of the $Pm\bar{3}n$-Nb_3Sn structure; the Sn atoms are shown in dark green, the Nb atoms in purple.

above, both AlH_3 and ZrH_3 found that the $Pm\bar{3}n$ symmetry is theoretically stable at high pressure. Thus, we start by calculating a pressure of 100 GPa. As a consequence, Al/Zr-substituted metal trihydride can be obtained from the ground-state structure. With this in mind, Matthias' sixth rule paves the way for a successful search for new superconducting materials, and one of them indicated the first rule that high symmetry is good and cubic symmetry is the best[26]—for example, sulfur hydride SH_3 has the $Im\bar{3}m$ symmetry with T_c of 203 K at a pressure of 155 GPa[9,27,28] and lanthanum hydride LaH_{10} the $Fm\bar{3}m$ symmetry with T_c of 260 K at a pressure of 185 GPa.[29−31] Herein, all compositions predict up to 92 structures, and we find that $Al_{0.5}Zr_{0.5}H_3$ is a simple cubic structure with $Pm\bar{3}$ symmetry. Following this, $Al_{0.5}Zr_{0.5}H_3$ does not decompose into the composition of AlH_3 and ZrH_3. This in turn implies that $Al_{0.5}Zr_{0.5}H_3$ is thermodynamically and dynamically stable favored over the AlH_3 and ZrH_3 structures. Yet, in this paper, the T_c is carried out by the anisotropic Migdal−Eliashberg equation.[32,33] Consequently, it will lead to the discovery of quite interesting $Al_{0.5}Zr_{0.5}H_3$. The findings suggest that the T_c of $Al_{0.5}Zr_{0.5}H_3$ reaches 55.3 K at the pressure of 100 GPa.

COMPUTATIONAL DETAILS

The search for the structures of Al/Zr-substituted metal trihydride was performed by CE, based on first-principle calculations. Substitution of the atomic type can be obtained from the CE method, indicating the energy of cluster expansion as a function of occupation. Al/Zr-substituted metal trihydride was explored by CE[34] with the MIT Ab initio Phase Stability (MAPS) code,[35] as implemented in the Alloy-Theoretic Automated Toolkit (ATAT)[35] with the combined Quantum Espresso (QE) package,[36] which plays a considerable role in the exploration of the derived ground-state structure. The plane-wave energy cutoff of 60 Ry and k-point meshes with about 4000 k-points were used. A plane-wave basis set up to cutoff energy of 500 eV and an initial Brillouin-zone (BZ) sampling grid of 8 × 8 × 8 k-points were used for the partial electronic band structure and density of state as implemented in the Vienna ab initio simulation package (VASP).[37] The zero-point energy of nuclei (ZPE) is estimated within the harmonic approximation, as employed with the use of PHONOPY package[38] with the combined QE package. For electron−phonon and the spectral function calculations a plane-wave energy cutoff of 60 Ry was used. The dense k-point mesh containing all k and k+q grid points was used. The subsequent electron−phonon and spectral function calcula-

https://doi.org/10.1021/acsomega.2c02447
ACS Omega 2022, 7, 28190−28197

tions depended on the k-point part because it covered the grid of the q-point. The calculations were computed in the first BZ on 16 × 16 × 16 k-points mesh and 4 × 4 × 4 q-meshes, showing that it is sufficient to produce accurate electron−phonon coupling. Computational details of the electron−phonon and spectral function calculations were successfully reported in the theoretical studies[19,20] The Allen−Dynes modified McMillan (ADM) equation[39] was exploited with the effective Coulomb pseudopotential parameter μ^* of 0.10−0.13 as follows

$$T_c = f_1 f_2 \frac{\omega_{\log}}{1.2} \exp\left[-\frac{1.04(1+\lambda)}{\lambda - \mu^*(1+0.62\lambda)}\right] \quad (1)$$

where $\omega_{\log}$ is the logarithmic average of the spectral function, λ is the total electron−phonon coupling strength, and f_1 and f_2 are the correction factors:

$$f_1 = \left\{1 + \left[\frac{\lambda}{2.46(1+3.8\mu^*)}\right]^{3/2}\right\}^{1/3} \quad (2)$$

$$f_2 = 1 + \frac{\lambda^2(\omega_2/\omega_{\log} - 1)}{\lambda^2 + [1.82(1+6.3\mu^*)(\omega_2/\omega_{\log}]^2} \quad (3)$$

More details about these equations are described in ref 39. In this methodology, the calculations were performed by using density functional theory (DFT). We used the ultrasoft pseudopotentials[40] and the generalized gradient approximation of the Perdew−Burke−Ernzerhof (GGA-PBE) functional[41] to describe the core and valence electrons as well as the conjugate gradient scheme, as implemented in the QE package.[36] We calculated the EPC within the density functional perturbation theory.[39,42] We investigated the nature of the superconducting gap by using anisotropic Migdal−Eliashberg (ME) formalism[32,33] with the electron−phonon coupling using the Wannier functions (EPW) software.[43−45] Generating maximally localized Wannier functions was used, as implemented in the WANNIER90 code.[46] The dense k-points mesh contained all k and k+q grid points were used. The calculates used a homogeneous fine k-point and q-point grid containing 60^3 points and 30^3 points, respectively, indicating that the calculations depended on the k-point part due to it covered the grid of q-point. We have studied the phonon-mediated superconductivity, and an effective Coulomb potential μ^* = 0.10 was used for solving the anisotropic ME equations

$$Z(\vec{k}, i\omega_n) = 1 + \frac{\pi T}{N_F \omega_n} \sum_{n'k'} \frac{\omega_n'}{\sqrt{\omega_n'^2 + \Delta^2(\vec{k}' i\omega_n')}} \lambda(\vec{k}, \vec{k}', n-n')\delta(\epsilon_k') \quad (4)$$

$$Z(\vec{k}, i\omega_n)\Delta(\vec{k}, i\omega_n) = \frac{\pi T}{N_F} \sum_{n'k'} \frac{\Delta(\vec{k}' i\omega_n')}{\sqrt{\omega_n'^2 + \Delta^2(\vec{k}' i\omega_n')}} [\lambda(\vec{k}, \vec{k}', n-n') - N_F V(\vec{k} - \vec{k}')]\delta(\epsilon_k') \quad (5)$$

$$\lambda(\vec{k}, \vec{k}', \omega) = \int_0^\infty d\omega \frac{2\omega}{(\omega_n - \omega_n')^2 + \omega^2} \alpha^2 F(\vec{k}, \vec{k}', \omega) \quad (6)$$

The T_c can be obtained from the superconducting gap $\Delta(i\omega_n)$ when numerically solving the ME equation.

RESULTS AND DISCUSSION

As first step, we aimed to search the Al/Zr-substituted metal trihydride structure at the pressure of 100 GPa. As mentioned previously, the CE was carried out for prediction of the ground-state structure, based on the DFT. In detail, a substitute for an atomic type was generated for up to 92 structures. All structures were confirmed by the ground-state energy based on the DFT. With this result, we found that the $Al_{0.5}Zr_{0.5}H_3$ structure is energetically more stable than the AlH_3 and ZrH_3 structures as shown in Figure 1a. Following this, we considered that the formation energy in the $Al_{0.5}Zr_{0.5}H_3$ structure might not be enough for confirmation of the structural stability. We further investigated the thermodynamic stablity by including the *PV* term; this in turn implies that the thermodynamic stability of the $Al_{0.5}Zr_{0.5}H_3$ structure is demonstrated by enthalpy. Moreover, the hydrogen is the light mass and it exhibits high frequency; therefore, the inclusion of ZPE plays an important role for examination of a stable structure. In the same way, our enthalpy calculations included the ZPE effect in the final calculations of a convex hull of different pressures. This is evident from Figure 1b, where it seems that the $Al_{0.5}Zr_{0.5}H_3$ structure is thermodynamically stable at the pressure of 100 GPa. Beyond 100 GPa up to 200 GPa, it shows that the $Al_{0.5}Zr_{0.5}H_3$ structure is thermodynamically stable up to at least 200 GPa. Additionally, it should be noted that type of high-pressure formation route can be demonstrated by considering A + B → C, where A and B are reactants and C is the resultant. At this point, we defined A and B as AlH_3 and ZrH_3; therefore, we can obtain the resultant from the high-pressure formation route, i.e., $(0.5)AlH_3 + (0.5)ZrH_3 \rightarrow Al_{0.5}Zr_{0.5}H_3$. The optimized structural parameters for the $Al_{0.5}Zr_{0.5}H_3$ structure are $a = b = c = 3.2773$ Å, with Al atoms located at the 1b symmetry site (0.000, 0.000, 0.000), Zr atoms located at the 1a symmetry site (0.500, 0.500, 0.500), and H atoms located at the 6g symmetry site (0.500, 0.000, 0.739); see Figure 1c. Apart from this, it should be mentioned that the space group of the AlH_3 and ZrH_3 structures is an isostructural of the Nb_3Sn structure with $Pm\bar{3}n$ symmetry, which are known crystal structures in the previously reported A15-group, as shown in Figure 1d. Subsequently, as mentioned in optimized structural parameters, our results manifested that a space group of the crystal structure of $Al_{0.5}Zr_{0.5}H_3$ is $Pm\bar{3}$ symmetry. With this, the $Al_{0.5}Zr_{0.5}H_3$ structure has lower symmetry than the AlH_3 and ZrH_3 structures through structural relaxation. This in turn implies that structural relaxation reduces from $Pm\bar{3}n$ symmetry to $Pm\bar{3}$ symmetry.

Regarding the electronic properties in the $Al_{0.5}Zr_{0.5}H_3$ structure, according to the aforementioned theoretical findings,[23] the existence of superconductivity in aluminum hydrides showed that a key factor is the contribution of the density of state. As demonstrated in Figure 2, we now move to the characteristic of the partial electronic structure and the partial density of state (PDOS) of the $Pm\bar{3}$ structure, and the present results show that the $Pm\bar{3}$ structure displays the metallicity at the pressure of 100 GPa. It found that the band dispersions are displayed by the weaving of the up-running bands from below E_f and down-running bands above E_F. It is a remarkable result that shows the valence and conduction bands are crossed around the Fermi level. Also, it is interesting to note that Zr substitution onto Al exhibits hybridization with the Al and H atoms, showing the PDOS. Here again, as already

https://doi.org/10.1021/acsomega.2c02447
ACS Omega 2022, 7, 28190−28197

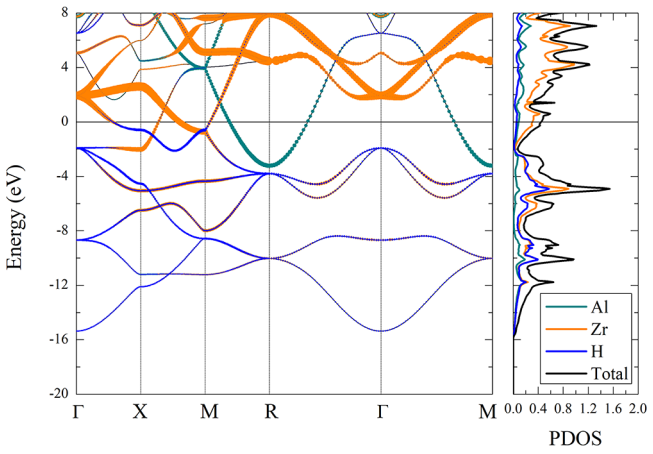

Figure 2. Calculated (left) partial electronic band structure and (right) partial density of states at a pressure of 100 GPa.

mentioned in the work of Abe,[23] the dominant feature of the occupied electron around the Fermi level toward the metallicity, supporting the T_c. As a result, our calculation manifested that the total DOS at the Fermi energy is larger in the $Al_{0.5}Zr_{0.5}H_3$ structure because of the dominant feature of the occupied electron of Zr around the Fermi level. To elucidate whether electronic PDOS at the Fermi level plays a crucial role in determining the corresponding superconducting behavior of the $Al_{0.5}Zr_{0.5}H_3$ structure, we must further consider their local density of states (LDOS), which is defined as

$$N(E, \mathbf{r}) = \sum_n \int \frac{d^3k}{(2\pi)^3} \delta(E - \epsilon_{nk}) |\psi_{nk}(\mathbf{r})|^2 \quad (7)$$

where $\psi_{nk}(\mathbf{r})$ and ϵ_{nk} indicate the Kohn−Sham eigenfunctions and eigenvalues of the system, respectively. As determined at the Fermi level, LDOS is a tool by which the degree of the electron−phonon coupling effect in a given material, directly giving rise to Cooper pairing, is visualized,[47,48] and the electron−phonon coupling effect will be discussed shortly later.

As mentioned earlier, the role of total DOS is a key factor in determining the electron−phonon coupling and superconducting transition temperature. It is also interesting to consider the lattice parameter and bond length with increasing pressure. The structural morphology has been compressed from 100 to 200 GPa. It showed that the lattice parameter decreased significantly by approximately 3.2773 to 3.09354 Å leading to decreasing a bond length. To explain, the bond length environment of the $Al_{0.5}Zr_{0.5}H_3$ structure displayed that d_{Al-H}, d_{Zr-H}, and d_{H-H} decreased moderately from 1.8173 to 1.7075 Å, from 1.8473 to 1.7523 Å, and from 1.5714 to 1.4465 Å, respectively, as shown in Figure 3. As a consequence, the remarkable result of total DOS showed that it declined steeply from 0.4388 to 0.4054 state/eV. To support the electron−phonon coupling of the $Al_{0.5}Zr_{0.5}H_3$ structure, it might be worth trying to estimate the electron−phonon coupling constant; namely, it is found to be possible that the electron−phonon coupling constant decreased with increasing pressure.

We now move to discuss the dynamical stability of the $Al_{0.5}Zr_{0.5}H_3$ structure. Our calculations showed that the $Al_{0.5}Zr_{0.5}H_3$ structure is dynamically stable from 100 to 200 GPa as the phonon frequencies are all positive, as shown in Figure 4a−c. These findings indicate the $Al_{0.5}Zr_{0.5}H_3$ structure can synthesize. What's more, it is interesting to note that the magnitude of the electron−phonon coupling constant, which represents a solid circle, can be decomposed into the phonon dispersion. Following this, the electron−phonon coupling constant exhibited the major contribution from the intermediate optical phonon mode to the optical phonon mode. This is in fact in line with the spectral function α^2F, as shown in Figure 4d−f. Here, it showed that the Eliashberg spectral function contributed slightly in acoustic phonon mode and it contributed mainly in the intermediate optical phonon mode as well as contributed moderately in the optical phonon mode. The solution of the integration of λ displayed that it climbed dramatically in the intermediate optical phonon mode. After that, it remained stable until the optical phonon mode. Then it increased moderately up to the highest phonon frequency of

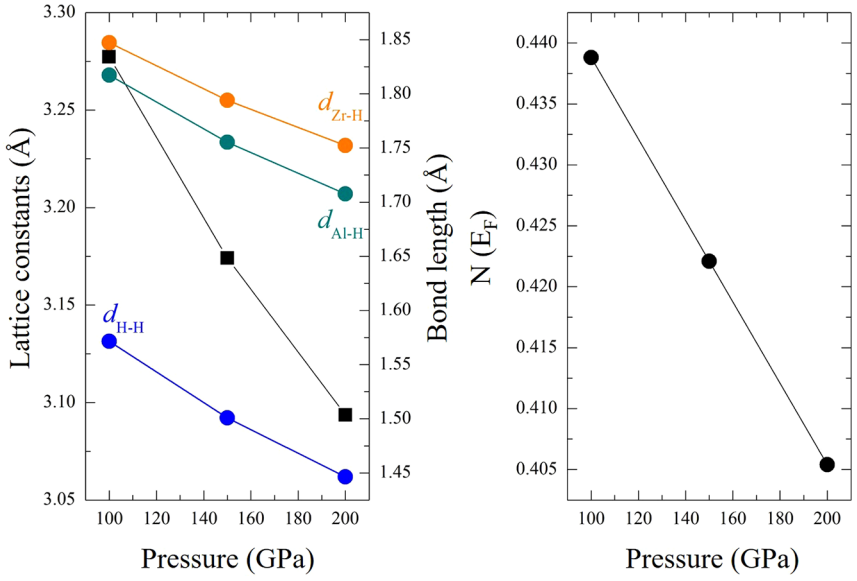

Figure 3. (Left) Calculated lattice constant and bond length as a function of pressure. (Right) Total density of states at Fermi level as a function of pressure ranging from 100 to 200 GPa.

https://doi.org/10.1021/acsomega.2c02447
ACS Omega 2022, 7, 28190−28197

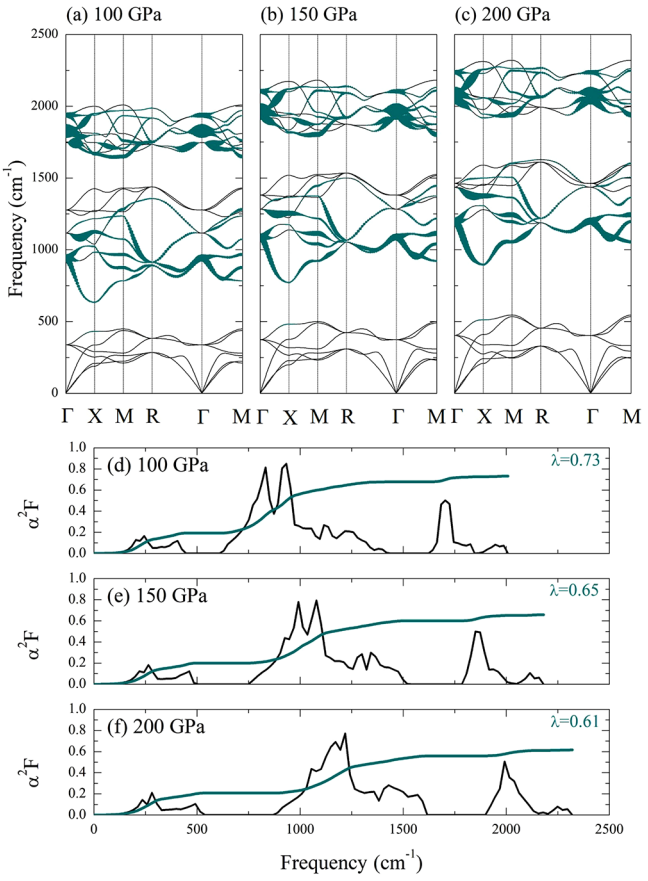

Figure 4. Calculated phonon dispersion at (a) 100 GPa, (b) 150 GPa, and (c) 200 GPa; the dark cyan circles represent the magnitude of electron−phonon coupling. The spectral function as a function of frequency (the black line) (d) 100 GPa, (e) 150 GPa, and (f) 200 GPa where the dark cyan line represents the cumulative λ.

each pressure, showing the integration of λ is 0.73, 0.65, and 0.61, respectively. To further understand the contribution of the intermediate optical phonon modes, arising particularly from the electron−phonon coupling, it is worth noting that a λ is highest at the intermediate optical phonon modes. Following this, we found that λ reached 0.484 at the pressure of 100 GPa. Moreover, on compression, λ is estimated to be 0.400 at a pressure of 150 GPa. On further compression to 200 GPa, the estimated λ reaches about 0.351. This in turn implies that λ is decreased with increasing pressure, making the estimated T_c is decrease from the influence of the contribution of the intermediate optical phonon modes. As the electron−phonon coupling constant is less than 1.5, the ADM equation is reduced to

$$T_c = \frac{\omega_{log}}{1.2} \exp\left[-\frac{1.04(1+\lambda)}{\lambda - \mu^*(1+0.62\lambda)}\right] \quad (8)$$

Here, we found that ω_{log} is 963 K and the T_c is 37 K, using μ^*= 0.10 at a pressure of 100 GPa. Additionally, the T_c is estimated by directly solving the McMillan formula with Allen−Dynes corrections μ^*= 0.13. The calculated T_c result shows that the estimated T_c is 28.8 K. This indicates that T_c is likely to be lower in μ^*= 0.13 than in μ^* = 0.10. Moreover, we found that the T_c is decreased with increasing pressure by using μ^* of 0.10−0.13.

To further explore the superconductivity of the $Al_{0.5}Zr_{0.5}H_3$ structure, the T_c is carried out by using the anisotropic ME equations. Herein, the anisotropic ME equations have been studied by considering the temperature dependence of the superconducting gap. Consequently, as can be seen in Figure 5,

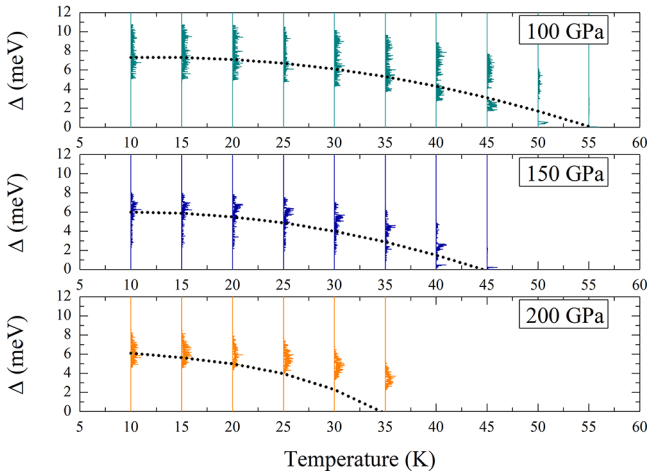

Figure 5. Anisotropic superconducting gap Δ as a function of temperature at pressures of 100, 150, and 200 GPa; the dot line represents superconducting gap Δ*v*alues, estimated using the isotropic Migdal-Eliashberg formalism.

we have shown the superconducting gap at the pressure of 100 GPa. Based on μ^* = 0.10, the superconducting gap closes at the critical temperature of 55.3 K. Likewise, at the pressure of 150 GPa, the superconducting gap displays the temperature evolution, indicating that the gap closes at the critical temperature estimated to be 45 K. With increasing pressure up to 200 GPa, the superconducting gap is likely to close at a critical temperature of 35 K. It should mention that the superconducting gap distribution shows a broad maximum around 4 meV, at which the superconducting gap is nearly zero. Therefore, the superconducting gap can be numerically solved by the anisotropic ME equations at each temperature. Following this, the superconducting gap closes at a critical temperature of 55.3 K, which plotted with the dot line, based on μ^*= 0.10, by using the isotropic ME theory. Likewise, beyond 100 GPa up to 200 GPa, the superconducting gap displays the temperature evolution, indicating that the gap closes at the critical temperature estimated to be 44.6 and 34.6 K, respectively. According to the aforementioned ADM findings, the results can guide as a characteristic that favors superconductivity. This in turn implies that the ADM and ME methods display a considerable decrease on the T_c from 150 to 200 GPa.

To this end, it is interesting to compare the superconducting properties of $Al_{0.5}Zr_{0.5}H_3$, AlH_3, and ZrH_3, respectively, as presented in Table 1. First, the qualitative prediction is theoretically confirmed by using first-principle calculation, based on phonon-mediated superconductivity. Note that $Al_{0.5}Zr_{0.5}H_3$ is found to be significantly higher in T_c than AlH_3 and ZrH_3 at the pressure of 100 GPa. Second, especially, the T_c qualitative prediction is quantitatively revealed by first-principle calculations with Migdal−Eliashberg theory. At the pressure of 100 GPa, there are noticeable increases in T_c. Following this, the T_c predicted in $Al_{0.5}Zr_{0.5}H_3$ is higher than AlH_3 and ZrH_3 by using the ADM and ME equations.

https://doi.org/10.1021/acsomega.2c02447
ACS Omega 2022, 7, 28190−28197

Table 1. Electron−Phonon Interaction and Logarithmic Averages of Phonon Frequencies of $Al_{0.5}Zr_{0.5}H_3$, AlH_3, and ZrH_3, Respectively[a]

	pressure (GPa)	λ	ω_{log}	μ^*	T_c (K)	method
$Al_{0.5}Zr_{0.5}H_3$[2]	100	0.73	963	0.1−0.13	37−28.8	ADM equation
$Al_{0.5}Zr_{0.53}$[2]	150	0.65	1049	0.1−0.13	30.1−22.2	ADM equation
$Al_{0.5}Zr_{0.53}$[2]	200	0.61	1091	0.1−0.13	26.2−18.6	ADM equation
$Al_{0.5}Zr_{0.53}$[2]	100	0.70	976	0.1−0.13	55.3−32.9	ME equation
$Al_{0.5}Zr_{0.53}$[2]	150	0.61	1103	0.1−0.13	44.6−29.6	ME equation
$Al_{0.5}Zr_{0.53}$[2]	200	0.73	849	0.1−0.13	34.6−16.3	ME equation
AlH_3[c]	105	0.71	852	0.13	28.5	isotropic Eliashberg
AlH_3[d]	110	0.74	852	0.14	24	McMilan equation
ZrH_3[e]	40	0.57	646	0.13	12.4	ADM equation

[a]The T_c's are calculated using the theoretical methods. A μ^* of 0.10−0.14 is used. [2]This work. [c]Reference 23. [d]Reference 25. [e]Reference 24.

Therefore, why was superconductivity predicted in $Al_{0.5}Zr_{0.5}H_3$ so high? To answer the question, as a possible cause of this, one might think of the intermediate optical phonon mode. Moreover, it should be stressed that both AlH_3 and ZrH_3 do not exhibit an intermediate optical phonon mode. This fact seems to indicate that the occurrence of intermediate optical phonon mode in the $Al_{0.5}Zr_{0.5}H_3$ structure may be important for the superconducting mechanism. In addition, it is worth mentioning that the anharmonic contribution to the magnitude of electron−phonon coupling as in AlH_3.[23,49] This because the anharmonic effect can weaken the electron−phonon coupling and can decrease λ with increasing pressure. Especially, in our case, one might think of the anharmonicity effect because the acoustic phonon mode is weakened by the magnitude of electron−phonon coupling.[23] What's more, it is interesting to note that the anharmonic contribution is not only effected on λ but also the T_c. Moreover, we demonstrated the anisotropic superconducting gap of $Al_{0.5}Zr_{0.5}H_3$ by considering $\mu^* = 0.13$. We found that the value of T_c decreased with respect to the value of T_c by adopting $\mu^* = 0.10$, as can be seen Figure 6. Additionally, our results show that $Al_{0.5}Zr_{0.5}H_3$ exhibits high T_c and is similar to those in ternary hydride $LiPH_6$ and $MgSiH_6$, where they indicate a possible way for achieving high-T_c evolution under high pressure.[50,51]

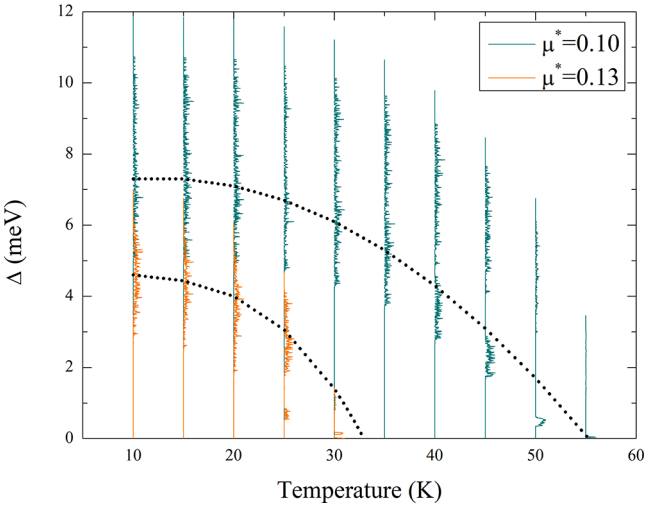

Figure 6. Anisotropic superconducting gap Δ, calculated by the effective Coulomb pseudopotential parameter, μ^*, of 0.10−0.13, as a function of temperature at a pressure of 100 GPa; the dotted line represents superconducting gap Δ values, estimated using the isotropic Migdal−Eliashberg formalism.

CONCLUSION

In summary, in this work, we identify the high-pressure phases of the $Al_{0.5}Zr_{0.5}H_3$ structure by performing the cluster expansion, based on the first-principle calculations. The CE demonstrates the $Al_{0.5}Zr_{0.5}H_3$ structure has the $Pm\bar{3}$ symmetry and the $Al_{0.5}Zr_{0.5}H_3$ structure is theoretically stable at high pressures. The value of T_c is higher in the anisotropic Migdal−Eliashberg equation. These findings suggest that the experimental observation of superconductivity should be expected by synthesizing the $Al_{0.5}Zr_{0.5}H_3$ structure. Finally, we point out that the existence of unexpected good symmetry can pave the way for further studies and research on the development of high-temperature superconductors.

AUTHOR INFORMATION

Corresponding Author

Thiti Bovornratanaraks − *Extreme Condition Physics Research Laboratory and Center of Excellence in Physics of Energy Materials (CE:PEM), Department of Physics, Faculty of Science, Chulalongkorn University, Bangkok 10330, Thailand; Thailand Center of Excellence in Physics, Ministry of Higher Education, Science, Research and Innovation, Bangkok 10400, Thailand;* orcid.org/0000-0001-6943-4032; Email: thiti.b@chula.ac.th

Authors

Prutthipong Tsuppayakorn-aek − *Extreme Condition Physics Research Laboratory and Center of Excellence in Physics of Energy Materials (CE:PEM), Department of Physics, Faculty of Science, Chulalongkorn University, Bangkok 10330, Thailand; Thailand Center of Excellence in Physics, Ministry of Higher Education, Science, Research and Innovation, Bangkok 10400, Thailand*

Rajeev Ahuja − *Materials Theory, Department of Physics and Astronomy, Uppsala University, SE-751 21 Uppsala, Sweden; Department of Physics, Indian Institute of Technology (IIT) Ropar, Rupnagar 140001 Punjab, India;* orcid.org/0000-0003-1231-9994

Wei Luo − *Materials Theory, Department of Physics and Astronomy, Uppsala University, SE-751 21 Uppsala, Sweden*

Complete contact information is available at: https://pubs.acs.org/10.1021/acsomega.2c02447

Notes

The authors declare no competing financial interest.

https://doi.org/10.1021/acsomega.2c02447
ACS Omega 2022, 7, 28190−28197

■ ACKNOWLEDGMENTS

This research project is supported by the Second Century Fund (C2F), Chulalongkorn University. This project is funded by the National Research Council of Thailand (NRCT): (NRCT5-RSA63001-04). This research is partially funded by Chulalongkorn University, Grant for Research. We gratefully acknowledge computational resources from the Swedish National Infrastructure for Computing. SNIC (2021/1-42). R.A. and W.L. acknowledge support from the Swedish Research Council (Grant no. VR-2020-04410) and Gust. Richert stiftelse, Sweden (2021-00665).

■ REFERENCES

(1) Matthias, B. T.; Geballe, T. H.; Geller, S.; Corenzwit, E. Superconductivity of Nb_3Sn. *Phys. Rev.* **1954**, *95*, 1435.
(2) Gavaler, J. R. Superconductivity in Nb−Ge films above 22 K. *Appl. Phys. Lett.* **1973**, *23*, 480−482.
(3) Ashcroft, N. W. Metallic Hydrogen: A High-Temperature Superconductor? *Phys. Rev. Lett.* **1968**, *21*, 1748−1749.
(4) Gilman, J. J. Lithium Dihydrogen Fluoride—An Approach to Metallic Hydrogen. *Phys. Rev. Lett.* **1971**, *26*, 546−548.
(5) Bardeen, J.; Cooper, L. N.; Schrieffer, J. R. Theory of Superconductivity. *Phys. Rev.* **1957**, *108*, 1175−1204.
(6) Ashcroft, N. W. Hydrogen Dominant Metallic Alloys: High Temperature Superconductors? *Phys. Rev. Lett.* **2004**, *92*, 187002.
(7) Zurek, E.; Hoffmann, R.; Ashcroft, N. W.; Oganov, A. R.; Lyakhov, A. O. A little bit of lithium does a lot for hydrogen. *Proc. Natl. Acad. Sci. U. S. A.* **2009**, *106*, 17640−17643.
(8) Strobel, T. A.; Goncharov, A. F.; Seagle, C. T.; Liu, Z.; Somayazulu, M.; Struzhkin, V. V.; Hemley, R. J. High-pressure study of silane to 150 GPa. *Phys. Rev. B* **2011**, *83*, 144102.
(9) Drozdov, A. P.; Eremets, M. I.; Troyan, I. A.; Ksenofontov, V.; Shylin, S. I. Conventional superconductivity at 203 K at high pressures in the sulfur hydride system. *Nature* **2015**, *525*, 73−76.
(10) Shamp, A.; Zurek, E. Superconducting High-Pressure Phases Composed of Hydrogen and Iodine. *J. Phys. Chem. Lett.* **2015**, *6*, 4067−4072. PMID: 26722778.
(11) Pépin, C. M.; Geneste, G.; Dewaele, A.; Mezouar, M.; Loubeyre, P. Synthesis of FeH5: A layered structure with atomic hydrogen slabs. *Science* **2017**, *357*, 382−385.
(12) Wang, H.; Tse, J. S.; Tanaka, K.; Iitaka, T.; Ma, Y. Superconductive sodalite-like clathrate calcium hydride at high pressures. *Proc. Natl. Acad. Sci. U. S. A.* **2012**, *109*, 6463−6466.
(13) Feng, X.; Zhang, J.; Gao, G.; Liu, H.; Wang, H. Compressed sodalite-like MgH6 as a potential high-temperature superconductor. *RSC Adv.* **2015**, *5*, 59292−59296.
(14) Abe, K.; Ashcroft, N. W. Stabilization and highly metallic properties of heavy group-V hydrides at high pressures. *Phys. Rev. B* **2015**, *92*, 224109.
(15) Peng, F.; Sun, Y.; Pickard, C. J.; Needs, R. J.; Wu, Q.; Ma, Y. Hydrogen Clathrate Structures in Rare Earth Hydrides at High Pressures: Possible Route to Room-Temperature Superconductivity. *Phys. Rev. Lett.* **2017**, *119*, 107001.
(16) Amsler, M. Thermodynamics and superconductivity of $S_xSe_{1-x}H_3$. *Phys. Rev. B* **2019**, *99*, 060102.
(17) Tsuppayakorn-aek, P.; Pinsook, U.; Luo, W.; Ahuja, R.; Bovornratanaraks, T. Superconductivity of superhydride CeH10 under high pressure. *Materials Research Express* **2020**, *7*, 086001.
(18) Sun, W.; Kuang, X.; Keen, H. D. J.; Lu, C.; Hermann, A. Second group of high-pressure high-temperature lanthanide polyhydride superconductors. *Phys. Rev. B* **2020**, *102*, 144524.
(19) Semenok, D. V.; Kruglov, I. A.; Savkin, I. A.; Kvashnin, A. G.; Oganov, A. R. On Distribution of Superconductivity in Metal Hydrides. *Curr. Opin. Solid State Mater. Sci.* **2020**, *24*, 100808.
(20) Di Cataldo, S.; von der Linden, W.; Boeri, L. Phase diagram and superconductivity of calcium borohyrides at extreme pressures. *Phys. Rev. B* **2020**, *102*, 014516.
(21) Tsuppayakorn-aek, P.; Phansuke, P.; Kaewtubtim, P.; Ahuja, R.; Bovornratanaraks, T. Enthalpy stabilization of superconductivity in an alloying S-P-H system: First-principles cluster expansion study under high pressure. *Comput. Mater. Sci.* **2021**, *190*, 110282.
(22) Tsuppayakorn-aek, P.; Phaisangittisakul, N.; Ahuja, R.; Bovornratanaraks, T. High-temperature superconductor of sodalite-like clathrate hafnium hexahydride. *Sci. Rep.* **2021**, *11*, 16403.
(23) Abe, K. Ab initio study of metallic aluminum hydrides at high pressures. *Phys. Rev. B* **2019**, *100*, 174105.
(24) Xie, H.; Zhang, W.; Duan, D.; Huang, X.; Huang, Y.; Song, H.; Feng, X.; Yao, Y.; Pickard, C. J.; Cui, T. Superconducting Zirconium Polyhydrides at Moderate Pressures. *J. Phys. Chem. Lett.* **2020**, *11*, 646−651. PMID: 31903761.
(25) Goncharenko, I.; Eremets, M. I.; Hanfland, M.; Tse, J. S.; Amboage, M.; Yao, Y.; Trojan, I. A. Pressure-Induced Hydrogen-Dominant Metallic State in Aluminum Hydride. *Phys. Rev. Lett.* **2008**, *100*, 045504.
(26) Conder, K. A second life of the Matthias's rules. *Supercond. Sci. Technol.* **2016**, *29*, 080502.
(27) Duan, D.; Liu, Y.; Tian, F.; Li, D.; Huang, X.; Zhao, Z.; Yu, H.; Liu, B.; Tian, W.; Cui, T. Pressure-induced metallization of dense (H 2 S) 2 H 2 with high-T c superconductivity. *Sci. Rep.* **2014**, *4*, 1−6.
(28) Einaga, M.; Sakata, M.; Ishikawa, T.; Shimizu, K.; Eremets, M. I.; Drozdov, A. P.; Troyan, I. A.; Hirao, N.; Ohishi, Y. Crystal structure of the superconducting phase of sulfur hydride. *Nat. Phys.* **2016**, *12*, 835−838.
(29) Somayazulu, M.; Ahart, M.; Mishra, A. K.; Geballe, Z. M.; Baldini, M.; Meng, Y.; Struzhkin, V. V.; Hemley, R. J. Evidence for Superconductivity above 260 K in Lanthanum Superhydride at Megabar Pressures. *Phys. Rev. Lett.* **2019**, *122*, 027001.
(30) Liu, H.; Naumov, I. I.; Hoffmann, R.; Ashcroft, N.; Hemley, R. J. Potential high-Tc superconducting lanthanum and yttrium hydrides at high pressure. *Proc. Natl. Acad. Sci. U. S. A.* **2017**, *114*, 6990−6995.
(31) Geballe, Z. M.; Liu, H.; Mishra, A. K.; Ahart, M.; Somayazulu, M.; Meng, Y.; Baldini, M.; Hemley, R. J. Synthesis and stability of lanthanum superhydrides. *Angew. Chem.* **2018**, *130*, 696−700.
(32) Migdal, A. Interaction between electrons and lattice vibrations in a normal metal. *Sov. Phys. JETP* **1958**, *7*, 996−1001.
(33) Eliashberg, G. Interactions between electrons and lattice vibrations in a superconductor. *Sov. Phys. JETP* **1960**, *11*, 696−702.
(34) Sanchez, J. M.; Ducastelle, F.; Gratias, D. Generalized cluster description of multicomponent systems. *Physica A: Statistical Mechanics and its Applications* **1984**, *128*, 334−350.
(35) Van De Walle, A.; Asta, M.; Ceder, G. The alloy theoretic automated toolkit: A user guide. *Calphad* **2002**, *26*, 539−553.
(36) Giannozzi, P.; et al. QUANTUM ESPRESSO: a modular and open-source software project for quantum simulations of materials. *J. Phys.: Condens. Matter* **2009**, *21*, 395502.
(37) Kresse, G.; Furthmüller, J. Efficient iterative schemes for *ab initio* total-energy calculations using a plane-wave basis set. *Phys. Rev. B* **1996**, *54*, 11169−11186.
(38) Togo, A.; Tanaka, I. First principles phonon calculations in materials science. *Scr. Mater.* **2015**, *108*, 1−5.
(39) Allen, P. B.; Dynes, R. C. Transition temperature of strong-coupled superconductors reanalyzed. *Phys. Rev. B* **1975**, *12*, 905−922.
(40) Vanderbilt, D. Soft self-consistent pseudopotentials in a generalized eigenvalue formalism. *Phys. Rev. B* **1990**, *41*, 7892−7895.
(41) Perdew, J. P.; Burke, K.; Ernzerhof, M. Generalized Gradient Approximation Made Simple. *Phys. Rev. Lett.* **1996**, *77*, 3865−3868.
(42) Baroni, S.; de Gironcoli, S.; Dal Corso, A.; Giannozzi, P. Phonons and related crystal properties from density-functional perturbation theory. *Rev. Mod. Phys.* **2001**, *73*, 515−562.
(43) Giustino, F.; Cohen, M. L.; Louie, S. G. Electron-phonon interaction using Wannier functions. *Phys. Rev. B* **2007**, *76*, 165108.
(44) Margine, E. R.; Giustino, F. Anisotropic Migdal-Eliashberg theory using Wannier functions. *Phys. Rev. B* **2013**, *87*, 024505.
(45) Poncé, S.; Margine, E.; Verdi, C.; Giustino, F. EPW: Electron−phonon coupling, transport and superconducting properties using

https://doi.org/10.1021/acsomega.2c02447
ACS Omega 2022, 7, 28190−28197

maximally localized Wannier functions. *Comput. Phys. Commun.* **2016**, *209*, 116−133.
(46) Mostofi, A. A.; Yates, J. R.; Lee, Y.-S.; Souza, I.; Vanderbilt, D.; Marzari, N. wannier90: A tool for obtaining maximally-localised Wannier functions. *Comput. Phys. Commun.* **2008**, *178*, 685−699.
(47) Heil, C.; Bachelet, G. B.; Boeri, L. Absence of superconductivity in iron polyhydrides at high pressures. *Phys. Rev. B* **2018**, *97*, 214510.
(48) Di Cataldo, S.; von der Linden, W.; Boeri, L. Phase diagram and superconductivity of calcium borohyrides at extreme pressures. *Phys. Rev. B* **2020**, *102*, 014516.
(49) Rousseau, B.; Bergara, A. Giant anharmonicity suppresses superconductivity in AlH 3 under pressure. *Phys. Rev. B* **2010**, *82*, 104504.
(50) Shao, Z.; Duan, D.; Ma, Y.; Yu, H.; Song, H.; Xie, H.; Li, D.; Tian, F.; Liu, B.; Cui, T. Ternary superconducting cophosphorus hydrides stabilized via lithium. *npj Computational Materials* **2019**, *5*, 104.
(51) Ma, Y.; Duan, D.; Shao, Z.; Yu, H.; Liu, H.; Tian, F.; Huang, X.; Li, D.; Liu, B.; Cui, T. Divergent synthesis routes and superconductivity of ternary hydride MgSiH 6 at high pressure. *Phys. Rev. B* **2017**, *96*, 144518.

https://doi.org/10.1021/acsomega.2c02447
ACS Omega 2022, 7, 28190−28197